A Letters Journal Exploring the Frontiers of Physics

April 2008

EPL, **82** (2008) 16002
doi: 10.1209/0295-5075/82/16002

www.epljournal.org

Pressure effects on the charge ordering in $Bi_{0.4}Ca_{0.6}MnO_3$ films of different orientation

J. Z. Wang[1], J. R. Sun[1(a)], W. Zhang[1], R. C. Yu[1], Y. Z. Chen[1], B. G. Shen[1] and W. B. Wu[2]

[1] *Beijing National Laboratory for Condensed Matter Physics, Institute of Physics, Chinese Academy of Sciences - Beijing 100080, PRC*
[2] *Hefei National Laboratory for Physical Sciences at the Microscale, University of Science and Technology of China - Hefei 230026, PRC*

received 22 November 2007; accepted in final form 5 February 2008
published online 18 March 2008

PACS 61.50.Ks – Crystallographic aspects of phase transformations; pressure effects
PACS 75.47.Lx – Manganites
PACS 73.50.-h – Electronic transport phenomena in thin films

Abstract – Effects of hydrostatic pressure on the charge ordering (CO) transition in the $Bi_{0.4}Ca_{0.6}MnO_3$ films respectively grown on (110) and (111) $SrTiO_3$ substrates have been experimentally studied. X-ray diffraction analysis indicates the occurrence of very differently deformed structures of the two films. Linear decrease of the CO temperature (T_{CO}) at different rates, ~ 12 K/GPa for the (110)-film and ~ 19 K/GPa for the (111)-film, is observed. Accompanying the depression of T_{CO}, partial melting of the charge-ordered phase occurs above a threshold pressure, $\sim 0.8/1.2$ GPa for the (111)/(110)-film. Analysis of the relative volume fraction of the CO phase, obtained based on the effective medium theory, shows that the CO collapsing occurs in a wide pressure range, typically ~ 1.2 GPa in width, and there will be no long-range CO phase above the pressure of $\sim 2/2.3$ GPa for the (111)/(110)-film. There is an exact correspondence between the CO melting and the pressure-driven upturn of resistivity above T_{CO}, suggesting the simultaneous occurrence of CO melting and shear-type lattice distortion. Different lattice strains are believed to be the reason for the dissimilar behaviors of the two films.

Colossal magnetoresistance, colossal electroresistance, and the diverse behaviors associated with phase separation are manifestations of the intricate relation between orbital, spin, charge and lattice degrees of freedom in manganites [1]. Due to the strong competition between Jahn-Teller (JT) effect, superexchange and double exchange interactions, a periodic arrangement of Mn^{4+} and Mn^{3+} can occur below a critical temperature T_{CO} in certain manganites [1,2]. Accompanying the charge ordering (CO) transition, a dramatic change in the magnetic and electronic properties of manganites appear [3,4]. There is also evidence that the charge-ordered state can be drastically modified by external perturbations such as magnetic field, pressure, and X-ray or visible-light illumination [5,6]. The complex pressure effect is of special interest. It has been found that high pressure can either depress or enhance the CO state and, sometimes causes a transition from the CO state to an A-type antiferromagnetic state [6]. Deformations of the MnO_6 octahedra under high pressure are believed to be the reason for these distinct behaviors of manganites.

Because of the presence of lattice strain, the CO state in thin films is severely depressed, and most of the previous studies of the CO effects have focused on bulk manganites. Fortunately, recent work showed that stable charge-ordered state could be obtained by growing the $Bi_{0.4}Ca_{0.6}MnO_3$ (BCMO) film on (110)-oriented $SrTiO_3$ substrates [7]. It was argued that when the (110)-orientation is adopted only the (001) axis of the film was clamped by substrate, and as a result, a cooperative JT distortion required by the CO transition is available. These results make possible a further study on the CO effects in manganite films.

We noticed that the evolution of the CO state under high pressures in thin films has not been fully studied. Compared with bulk materials, thin films are distinct in many aspects. By carefully choosing the crystal orientation of substrate, the structure deformation of the film

(a) E-mail: jrsun@g203.iphy.ac.cn

can be tuned, obtaining the state unavailable by other techniques. Furthermore, because of the substrate-induced structure deformation, the films are actually in an unstable state due to the increase of, for example, elastic energy, which may make the films sensitive to external perturbations. As a result, the pressure effect in thin films is expected to bear some special features considering its influence on the subtle balance between competitive mechanisms in the deformed films. Based on this consideration, in this paper we performed a comparable study of the influence of hydrostatic pressure on the CO of BCMO films with different crystal orientations. It is found that the films on differently orientated substrates, thus dissimilar lattice strains, exhibit significantly different pressure effects. It is further found that the pressure not only depresses $T_{\rm CO}$ but also causes a collapse of the CO state.

Two BCMO film were respectively prepared on a (110) and a (111) $SrTiO_3$ substrate of the dimension $6\times3\times0.5\,\mathrm{mm}^3$ by the pulsed-laser ablation technique from a ceramic target with the nominal composition $Bi_{0.4}Ca_{0.6}MnO_3$. During the deposition, the substrate temperature was kept at $\sim700\,^\circ$C and the O_2 pressure at $\sim60\,$Pa. The film thickness is $\sim150\,$nm, determined by a DEKTAK-3 Surface Profile Measuring System. Energy-dispersive X-ray spectroscopy (EDX) analyses detect the composition $\mathrm{Bi:Ca:Mn}\approx0.41:0.59:1$ for both films, obtained by averaging the data of 14 different locations on the film plane.

Transport measurements were performed on a Mag-Lab EXA System (2000 Oxford UK). The standard four-point technique, with silver-paint electric contacts, has been used. The hydrostatic pressure, calibrated at ambient temperature with a manganin coil, was provided by a clamp-type piston cylinder cell with the pressure-medium of 1 : 1 silicone oil and kerosene. The temperature was monitored by a NiCr-NiAl thermocouple placed near the sample. All of the resistive data presented here were collected in the warming process.

Both films are epitaxially grown, as confirmed by the four-circle X-ray diffraction measurements. In fig. 1 we show the XRD spectra of the (110)/(111)-BCMO film, where the reflections are from the $(n00)$ planes and $(nn0)/(nnn)$ planes. Based on the XRD analyses, the lattice parameters can be obtained, and they are $a=b=3.787\,$Å, $c=3.836\,$Å with $\alpha\approx90.5^\circ$ for the (110)-film, which are in agreement with the results previously reported for a similar film [7], and $a=b=3.832\,$Å, $c=3.704\,$Å for the (111)-film. Compared with the bulk BCMO above the CO transition ($a=b=3.81\,$Å, $c=3.79\,$Å) [8], the (110)-film exhibits a slightly deformed tetragonal structure with an obviously elongated c-axis and a shrunk a-b plane. The assumption that cell volume keeps nearly constant when it is deformed has been adopted in determining c for the (110)-film. The (111)-film has not been studied before, and the lattice constants obtained here are similar to those of the bulk BCMO in the charge-ordered state. The deviation from cubic symmetry of the crystal

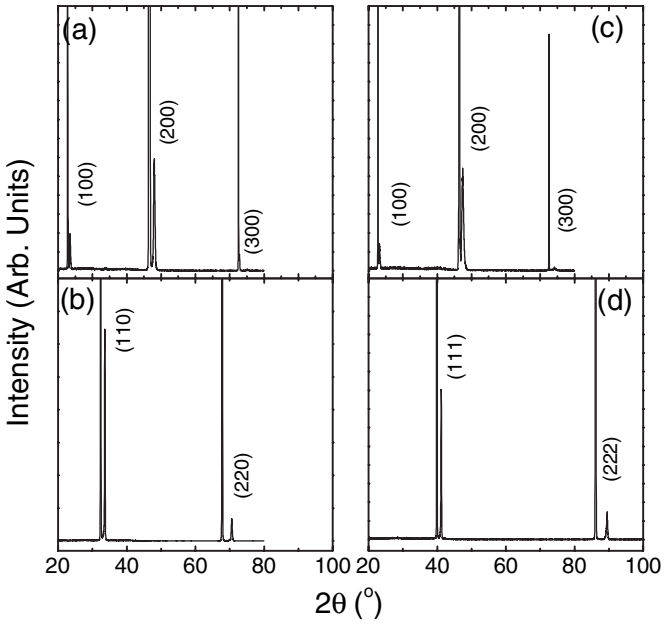

Fig. 1: X-ray diffraction spectrum of the $(n00)$ and $(nn0)/(nnn)$ planes of the (110) (left)/(111) (right)-BCMO film.

structure can be described by a so-called average distortion ratio defined as [9]

$$D=\frac{1}{3}\sum_{i=1}^{3}\left|\frac{a_i-\overline{a}}{a_i}\right|,$$

where $\overline{a}=(abc)^{1/3}$, $a_1=a$, $a_2=b$, and $a_3=c$. A direct calculation shows that $D\approx0.57\%$ for the (110)-film and $\sim1.4\%$ for the (111)-film ($D=0.23\%$ for the bulk BCMO without CO). The structure deformation is obviously larger for the latter film. Compared with the (110)-film, the peak profile of the $\theta-2\theta$ scan of the (111)-film is also broader. The full width at half height of the (200) peak is $\sim0.61^\circ$, while it is $\sim0.38^\circ$ for the (110)-film. This reveals the relatively poor crystallinity of the (111)-film, which is consistent with the results obtained in $Nd_{0.5}Sr_{0.5}MnO_3$ film [10].

Figure 2 shows the temperature dependence of resistivity measured under different pressures. Both films are insulating in the whole temperature range investigated. A visible resistive anomaly appears at $T_{\rm CO}\approx270\,$K for the (110)-film and $T_{\rm CO}\approx279\,$K for the (111)-film (inset plot in fig. 2), which is a signature of the CO transition by analogy with the bulk BCMO [11]. The periodic arrangement of Mn^{3+} and Mn^{4+} localizes charge carriers, thus enhances the resistivity below $T_{\rm CO}$. Compared with bulk BCMO, the CO temperature of the film is considerably low, $\sim270\,$K or $\sim279\,$K for the films and $\sim330\,$K for the bulk counterpart [11]. $T_{\rm CO}\approx270\,$K is similar to that previously reported for the (110)-BCMO film [8]. It would be instructive to note the completely different structure of the two films. The similarity of the structure of the (111)-film to bulk BCMO could favor the charge-ordered state,

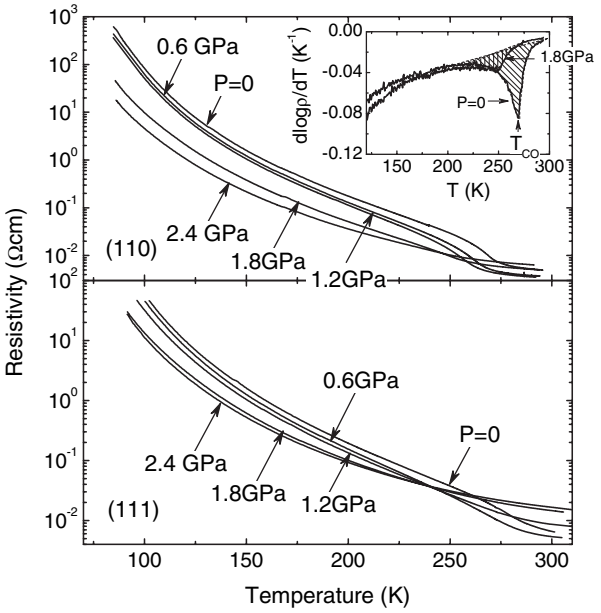

Fig. 2: Temperature dependence of the resistivity of BCMO films measured under different pressures. The inset plot shows the derivative of resistivity with respect to temperature. The hatched region sketches resistive anomaly caused by the CO transition.

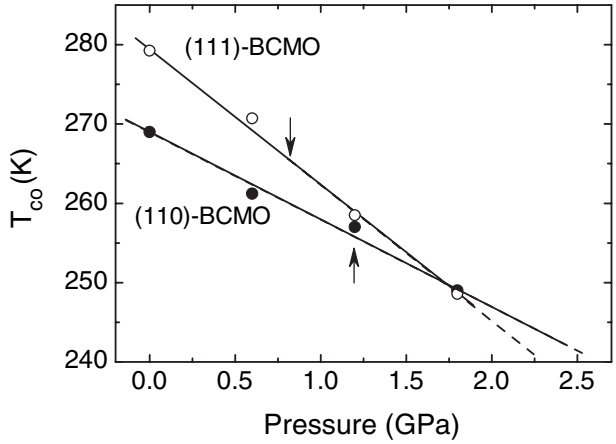

Fig. 3: Variation of transition temperature $T_{\rm CO}$ with applied pressure. Arrows in the figure mark the pressures where partial CO melting appears. Solid and dashed lines are guides for the eye.

while on the contrary, the poor crystallinity of the (111)-film may tend to depress CO. The occurrence of the CO transition in this film, though $T_{\rm CO}$ reduces from $\sim 330\,$K (for the bulk BCMO) to $\sim 279\,$K, could be a consequence of the competition between the two mechanisms. This is different from $Nd_{0.5}Sr_{0.5}MnO_3$, in which the CO state was completely destroyed by the poor crystal quality of the film [10].

Two obvious pressure effects can be identified from the data in fig. 2. The first one is the depression of the CO transition by applied pressure. $T_{\rm CO}$ varies from $\sim 270/279\,$K at $P=0$, to $\sim 248/255\,$K at $P=1.8/1.2\,$GPa, for the (110)/(111)-film (fig. 3). A direct calculation gives the decreasing rate $\mathrm{d}\ln T_{\rm CO}/\mathrm{d}P \approx -0.043\,\mathrm{GPa}^{-1}$ for the (110)-film and $-0.074\,\mathrm{GPa}^{-1}$ for the (111)-film, (*i.e.*, $\mathrm{d}T_{\rm CO}/\mathrm{d}P \approx 12\,\mathrm{K/GPa}$ and $19\,\mathrm{K/GPa}$), respectively. The former is only $\sim 58\%$ as large as the latter in magnitude. It seems easier for a pressure to modify the CO state of the (111)-film than that of the (110)-film. However, the charge-ordered state of the (111)-film is expected to be more insensitive to external perturbations because of its robustness demonstrated by the higher $T_{\rm CO}$ compared with the (110)-film. As revealed by the XRD analysis, the starting states of the two films are different, and the (111)-film is more severely deformed, which could be a reason for the different pressure effects observed. We will return to this problem later.

The second effect is the progressive collapse of the CO state above a critical pressure. To the best of our knowledge, a quantitative analysis about this process is still lacking even for bulk materials. As shown in the inset in fig. 2, accompanying the low-temperature shift of $T_{\rm CO}$, the resistive anomaly at $T_{\rm CO}$ is considerably weakened, which implies the occurrence of partial melting of the CO phase. In fact, the fraction of the CO phase can be obtained as a function of pressure based on a simple analysis. It may be a good approximation that the sample is in a well charge-ordered state well below $T_{\rm CO}$ without pressure, while completely charge-disordered under the pressure of 2.4 GPa. For $T < T_{\rm CO}$, the resistivity under an intermediate pressure is determined by the randomly distributed charge-ordered and charge-disordered domains, and can be described by the effective medium theory with an adjustable parameter $f_{\rm CO}$, the relative volume fraction of the CO phase [12]:

$$(1-f_{\rm CO})\left(\frac{\sigma_{\rm CO}^{1/t}-\sigma^{1/t}}{\sigma_{\rm CO}^{1/t}+A\sigma^{1/t}}\right)+f_{\rm CO}\left(\frac{\sigma_{\rm CDO}^{1/t}-\sigma^{1/t}}{\sigma_{\rm CDO}^{1/t}+A\sigma^{1/t}}\right)=0. \quad (1)$$

Considering the fact that the film is relatively thick, approximating it as a three-dimensional system could be acceptable, *i.e.* $t=2$. Where $A=(1-f_{\rm C})/f_{\rm C}$, $f_{\rm C}\approx 0.17$ is the threshold volume fraction for the percolation. $\sigma_{\rm CO}$ is the conductivity of charge-ordered phase, and it can be approximated by the conductivity without pressure. $\sigma_{\rm CDO}$ is the conductivity of charge-disordered phase in the case of $P=0$. It could be different from that under the pressure of 2.4 GPa, noting the considerable variation of resistivity under pressure. It is fortunate that pressure influences mainly the vertical offset of the $\log\rho - T$ curve, instead of the $\log\rho - T$ dependence (fig. 2). It is therefore reasonable to represent $\sigma_{\rm CDO}(T)$ with that under 2.4 GPa, after an appropriate vertical shift to align the high-temperature conductivity under different pressures.

With the $\sigma_{\rm CO}$ and $\sigma_{\rm CDO}$ being known, eq. (1) can be directly used to the calculation of the resistivity under

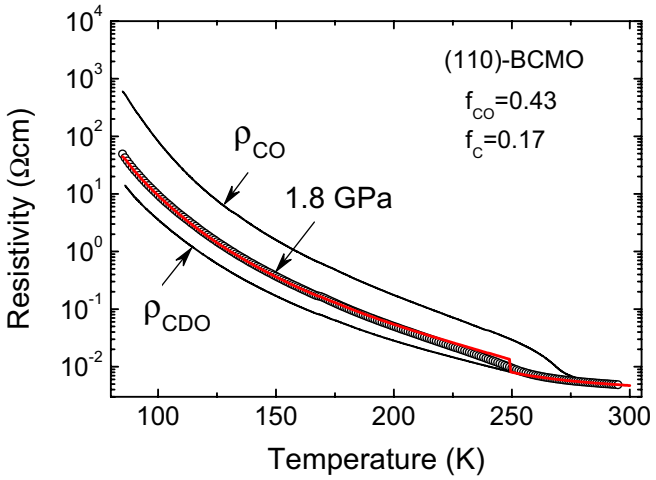

Fig. 4: (Color online) Comparison of observed (symbols) and calculated (red line) results. The parameters $f_C = 0.17$ and $f_{CO} = 0.43$ have been adopted for the calculation. Resistivities of the charge-ordered and charge-disordered phases are also shown (solid lines).

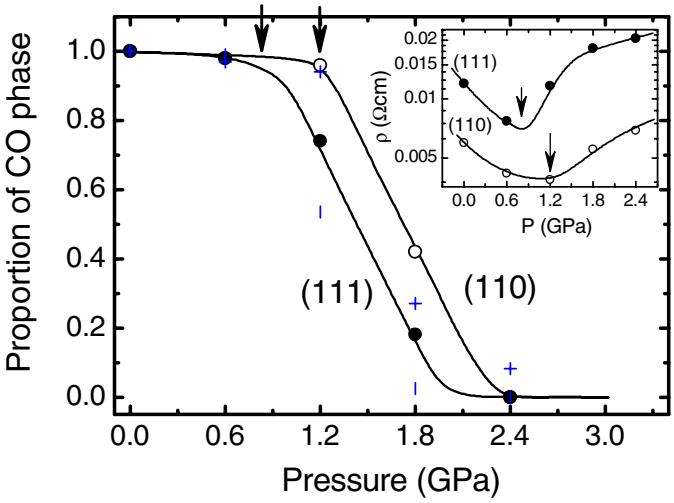

Fig. 5: (Color online) Relative volume fraction of the charge-ordered phase as a function of applied pressure obtained in the temperature range below 180 K. Colored crosses and bars are the normalized integral area of the $\mathrm{d}\log\rho(T)/\mathrm{d}T$) peak (illustrated in the inset of fig. 2) across T_{CO} for the (110)- and (111)-film, respectively. The inset plot shows the pressure dependence of resistivity at a fixed temperature $T = 280$ K. Arrows mark the correspondence between the CO melting and resistive upturn.

an arbitrary pressure between 0 and 2.4 GPa. The volume fraction of the CO phase f_{CO} is so chosen that it gives a satisfactory description to experiment results. Figure 4 is a comparison of the observed and calculated data. Only the results of $P = 1.8$ GPa are presented for clarity. It shows that the effective medium theory provides an excellent description for experiment results when the parameter $f_{CO} = 0.43$ is adopted. The discrepancy is within 2% in a wide temperature range below T_{CO}. The divergence near T_{CO} may arise from the assumption that f_{CO} is temperature-independent, which is reasonable only in the low-temperature range.

It would be instructive to analyze the variation of f_{CO} with applied pressure. Figure 5 exemplifies the proportion of the CO phase f_{CO} as a function of pressure obtained in the temperature range below 180 K (results are essentially the same in the temperature range from 100 K to 180 K). It shows the evolution of the fraction of the CO phase when T_{CO} decreases under the applied pressure. Different from T_{CO} which exhibits an instantaneous response to applied pressure, however, the CO melting occurs only above a threshold pressure, and proceeds in a wide pressure range of ~ 1.2 GPa. It begins when pressure exceeds ~ 0.8 GPa for the (111)-film and ~ 1.2 GPa for the (110)-film, and ends above the pressure of ~ 2 GPa and ~ 2.3 GPa for the (111)- and (110)-films, respectively. Again, the differences between the two films are shown here. It should be emphasized that despite the occurrence of partial melting of the CO phase, the general T_{CO}-P relation keeps unaffected (fig. 3). As an alternative, the resistive anomaly caused by the CO transition reflects the degree of charge ordering. Its decrease with increasing pressure implies the weakening of charge ordering. Thus the CO degree and/or population can also be measured by the integral area below the $\mathrm{d}\log\rho/\mathrm{d}T$ peak (inset in fig. 2), and similar results of the evolution of CO phase are obtained as shown in fig. 5 as well. Its disadvantage is that it is unable to describe charge ordering away from T_{CO}, while the data fitting based on the effective medium theory results in strict f_{CO} values below T_{CO}.

The pressure-driven broadening of the resistive transition associated with the CO has been observed in bulk materials. However, the present work reveals the presence of two different processes behind this phenomenon, which has not been explicitly pointed out before. The first one is the simple broadening of the phase transition due to, for example, the appearance of lattice strains and the second one is the partial melting of the CO phase. The latter process occurs only after a threshold pressure.

As a supplement, we would like to point out that f_{CO} is actually the volume fraction of the pressure-free phase. Considering the fact that the pressure-free phase is mainly charge-ordered, treating f_{CO} as the proportion of the charge-ordered phase would not affect the conclusion.

Due to the presence of structure deformation, the pressure effect for the films could be different from that for the bulk manganites in a thermal-equilibrium state considering the fact that external pressure can effectively affect the subtle balance between the competitive mechanisms in the deformed films. This implies that the different pressure effects of the two films and the special behaviors of the CO phase under applied pressure may have a close relation to the distinct structural property of the films and the evolution of structure deformation with the increase of pressure.

Because of the limitation of the experiment condition, the structure under high pressure has not been measured. It has recently been reported that the structure deformation of the manganite experienced a complex process, first decreasing then increasing with the increase of pressure. It was further proved that the JT-type distortion weakened while a shear-type distortion enhanced when pressure rose [13], and there was a minimum lattice distortion at the crossover pressure P^* from the former to the latter. The cooperative JT distortion and even the concomitant orbital ordering can be completely depressed above a critical pressure as reported in $LaMnO_3$ [14]. Resisitivity was found to exhibit a similar variation with structure deformation. Instead of monotonically decreasing, it displayed a significant upturn above the crossover pressure [15]. Moreover, this kind of pressure-driven minimum of resistivity appears to sustain at all temperatures, as found in $La_{0.6}Y_{0.07}Ca_{0.33}MnO_3$ [15], $Pr_{0.7}Ca_{0.3}MnO_3$ [16], etc. This result indicates that the resisitivity variation with pressure of the non-charge-ordered phase can provide indirect information on structure changes.

Complex resistivity variations are also observed in the BCMO films. Taking the (110)-film at 280 K as an example, as shown by the inset plot in fig. 5, it is $\sim 0.00596\,\Omega$cm without pressure, reduces to the minimum value of $\sim 0.00385\,\Omega$cm under the pressure of 1.2 GPa, upturns with further increasing pressure, and gets a value of $\sim 0.0069\,\Omega$cm under the pressure of 2.4 GPa. Similar behaviors are observed in the (111)-film except that the critical pressure for the appearance of resistivity minimum is significantly smaller (~ 0.8 GPa). This phenomenon reveals first a decrease then an increase of structure deformation of the film. In analogy with the previous work [13,15], the BCMO films may experience an evolution from JT-type to shear-type distortions at the pressure of ~ 0.8 GPa for the (111)-film and of ~ 1.2 GPa for the (110)-film. It is instructive to note the coincidence of the threshold pressures for the deformation crossover (marked by arrows in the inset in fig. 5) and the CO collapsing (marked by arrows in fig. 5). It is possible that as the JT-distortion weakens T_{CO} reduces, while the CO phase begins to melt only after the shear-type distortion appears. Compared with the bulk materials, the critical pressure is obviously low in the films. It is $P^* \sim 0.8$–1.2 GPa for BCMO films while $P^* \sim 7$ GPa and ~ 4 GPa for bulk $Nd_{0.5}Ca_{0.5}MnO_3$ [13] and $La_{0.6}Y_{0.07}Ca_{0.33}MnO_3$ [15], respectively. It may be an indication that the lattice strain imposed by substrate favors the shear-type lattice distortion.

In BCMO films, for $P < P^*$, it is the JT-type distortion of the MnO_6 octahedra that holds the CO phase. The resistance decreases for a decrease in the JT-type distortion under pressure. For $P > P^*$, the shear-type distortion begins to appear and its region may expand with increasing pressure. It retains to low temperature below T_{CO} and charge ordering cannot be formed in these regions. Thus phase separation appears with coexistence of charge ordering and charge-disordered phases under an arbitary pressure. In this case, two effects produced by the shear-type distortion can affect the electrical transport. The first one is that the shear distortion leads to an increase of resistivity as found in a nearly single electronic phase, such as in the charge-disordered state above T_{CO} of BCMO (inset of fig. 5), and in $La_{0.6}Y_{0.07}Ca_{0.33}MnO_3$, $Pr_{0.7}Ca_{0.3}MnO_3$, etc, due to a possible localization of conduction electrons. The second is that the shear-type distortion above P^* simultaneously melts a part of the highly insulating CO phase to semiconducting disorder, which lead to a pronounced decrease of resistance. Below T_{CO} above P^*, the two effects coexist and the second predominates, resulting in the observed decrease of resitivity with increasing pressure in fig. 2. With further increase of the pressure, the shear-type distortion strengthens and the collapsed region $(1 - f_{CO})$ widens up to a pressure high enough, $\sim 2/2.3$ GPa for the (111)/(110)-BCMO film, to deform the MnO_6 octahedra in a shear type totally and the charge ordering then can be completely depressed.

As for the different pressure effects in the (110)- and (111)-films, such as the different critical pressures, they could be ascribed to different structure deformations. Although both films exhibit a slightly deformed tetragonal structure, the former is elongated while the latter is compressed along the c-axis compared with the non–charge-ordered bulk BCMO. The instability of the films due to, for example, the increase of elastic energy enhances the pressure effect. This phenomenon is especially obvious in the (111)-film, which displays a considerably large D value ($\sim 1.4\%$). The prior structure deformation in the films also advances the evolution from the JT-type to the shear-type deformation, as demonstrated by the lower crossover pressures compared with the bulk.

In summary, the effects of hydrostatic pressure on CO transition in $Bi_{0.4}Ca_{0.6}MnO_3$ films grown, respectively, on the (110) and the (111) $SrTiO_3$ substrate have been studied. Linear decrease of the CO temperature (T_{CO}) at different rates, ~ 12 K/GPa for the (110)-film and ~ 19 K/GPa for the (111)-film, has been observed. Accompanying the depression of T_{CO}, partial melting of the charge-ordered phase occurs above a critical pressure, $\sim 0.8/1.2$ GPa for the (111)/(110)-film. Analysis of the volume fraction of the CO phase, obtained based on the effective medium theory, shows that the CO collapsing occurs in a wide pressure range, typically ~ 1.2 GPa in width, and there will be no CO phase above the pressure of $\sim 2/2.3$ GPa for the (111)/(110)-film. There is an exact correspondence between the CO melting and the pressure-driven upturn of resistivity above T_{CO}, suggesting the simultaneous occurrence of CO melting and shear-type lattice distortion. Different lattice strains are believed to be the reason for the dissimilar behaviors of the two films.

* * *

This work has been supported by the National Natural Science Foundation of China and the National Basic Research of China.

REFERENCES

[1] For a review, see Tokura Y. (Editor), *Colossal Magnetoresistance Oxides* (Gordon and Breach, London) 1999; Dagotto E. (Editor), *Nanoscale Phase Separation and Colossal Magneto-resistance* (Springer, Berlin) 2002.
[2] Tokura Y. and Nagaosa N., *Science*, **288** (2000) 462.
[3] Biswas A., Raychaudhuri A. K., Mahendiran R., Guha A., Mahesh R. and Rao C. N. R., *J. Phys.: Condens. Matter*, **9** (1997) L355; Biswas A., Arulraj A., Raychaudhuri A. K. and Rao C. N. R., *J. Phys.: Condens. Matter*, **12** (2000) L101; Renner C., Aeppli G. and Ronnow H. M., *Mater. Sci. Eng. C*, **25** (2005) 775.
[4] Katsufuji T., Tanabe T., Ishikawa T., Yamanouchi S., Tokura Y., Kakeshita T., Kajimoto R. and Yoshizawa H., *Phys. Rev. B*, **60** (1999) R5097.
[5] Tomioka Y., Asamitsu A., Kuwahara H., Moritomo Y. and Tokura Y., *Phys. Rev. B*, **53** (1996) R1689; Kiryukhin V., Casa D., Hill J. P., Keimer B., Vigliante A., Tomioka Y. and Tokura Y., *Nature*, **386** (1997) 813.
[6] Tokura Y., Kuwahara H., Moritomo Y., Tomioka Y. and Asamitsu A., *Phys. Rev. Lett.*, **76** (1996) 3184; Moritomo Y., Kuwahara H., Tomioka Y. and Tokura Y., *Phys. Rev. B*, **55** (1997) 7549.
[7] Kim D. H., Christen H. M., Varela M., Lee H. N. and Lowndes D. H., *Appl. Phys. Lett.*, **88** (2006) 202503.
[8] Bokov V. A., Grigoryan N. A. and Bryzhina M. F., *Phys. Status Solidi*, **20** (1967) 745.
[9] Jirak Z., Krupica S., Simsa Z., Dlouha M. and Vratislav S., *J. Magn. & Magn. Mater.*, **53** (1985) 153.
[10] Nakamura M., Ogimoto Y., Tamaru H., Izumi M. and Miyano K., *Appl. Phys. Lett.*, **86** (2005) 182504.
[11] Woo H., Tyson T. A., Croft M., Cheong S.-W. and Woicik J. C., *Phys. Rev. B*, **63** (2001) 134412.
[12] Kim K. H., Uehara M., Hess C., Sharma P. A. and Cheong S. W., *Phys. Rev. Lett.*, **84** (2000) 2961.
[13] Arulraj A., Dinnebier R. E., Carlson S., Hanfland M. and van Smaalen S., *Phys. Rev. Lett.*, **94** (2005) 165504.
[14] Loa I., Adler P., Grzechnik A., Syassen K., Schwarz U., Hanfland M., Rozenberg G. Kh., Gorodetsky P. and Pasternak M. P., *Phys. Rev. Lett.*, **87** (2001) 125501.
[15] Cui C. W., Tyson T. A., Zhong Z., Carlo J. P. and Qin Y. H., *Phys. Rev. B*, **67** (2003) 104107.
[16] Cui C. W. and Tyson T. A., *Appl. Phys. Lett.*, **83** (2003) 2856.